Ultrafine high performance polyethylene fibers

Ultrafine High Performance Polyethylene Fibers

*Jay H. Park, and Gregory C. Rutledge**

Department of Chemical Engineering, Massachusetts Institute of Technology

77 Massachusetts Ave. Cambridge, MA, 02139, USA

Abstract

Stiff, strong and tough ultrafine polyethylene fibers that rival the best high performance fibers, but with diameters less than one micron, are fabricated for the first time by "gel-electrospinning". In this process, solution concentration and process temperatures are chosen to induce the formation of gel filaments "in flight", which are subsequently drawn at high rates as a consequence of the whipping instability. The resulting submicron diameter fibers exhibited Young's moduli of 73 ± 13 GPa, yield strengths of 3.5 ± 0.6 GPa, and toughnesses of 1.8 ± 0.3 GPa, on average. Among the smallest fibers examined, one with a diameter of 490 ± 50 nm showed a Young's modulus of 110 ± 16 GPa, ultimate tensile strength of 6.3 ± 0.9 GPa, and toughness of 2.1 ± 0.3 GPa, a combination of mechanical properties that is unparalleled among polymer fibers to date. The correlation of stiffness, strength and toughness with fiber diameter is attributed to high crystallinity and crystallite orientation, combined with fewer defects and enhanced chain slip associated with small diameter and high specific surface area. Gel-electrospinning improves the prospects for production of such fibers at scale.

Keywords: electrospinning; polyethylene; modulus; strength; toughness; nanofiber

Introduction

Over the past two decades, electrospinning has attracted much interest from the academic and industrial scientific communities due to its capability for continuous fabrication of ultrafine fibers having diameters from tens of nanometers to a few microns[1] (commonly known as "nanofibers"). Unlike conventional fiber spinning processes, the fabrication of these submicron fibers is driven by electrical forces rather than mechanical forces, and can involve high uniaxial extensional strain rates, up to 1000 s^{-1}.[2] These fibers can be produced from a wide range of organic materials and inorganic precursors, and typically have high specific surface areas, as a result of their nanometer-scale fiber diameters. The structural and functional versatility of these fibers has allowed a remarkably broad range of applications, such as membranes and filters,[3-6] battery materials,[7-9] sensors,[10-12] biomaterials,[13-15] and drug delivery.[16,17]

In each application, the mechanical integrity of the electrospun material ultimately determines whether it will hold up under end-use conditions, involving exposure to environmental contamination, thermal or mechanical cycling, or inter-laminar abrasion in fabricated devices. Typical Young's moduli of submicron-diameter electrospun fibers range from about 0.1 GPa to 10 GPa,[18-20] which are larger than those of the bulk materials, but still smaller than most conventional polymer fibers.[21] This deficiency becomes especially clear when compared to engineered high performance fibers, like Kevlar®, Twaron®, Dyneema® or Spectra®, that exhibit Young's moduli of 100 GPa or higher. If these ultrafine fibers are ever to find application in high performance applications like transparent composites, soft body armor, industrial protective clothing or structural cords and ropes, significant increases in stiffness, strength, and toughness of these fibers are required.

Numerous recent studies have shown that a 3- to 5-fold increase of the fiber modulus can be observed with decreasing diameters below about 500 nm.[22-25] Such improvements in stiffness are generally related to high levels of molecular orientation within the thinnest fibers.[22, 26] Some groups have explained the origin of this molecular orientation in terms of a surface oriented layer,[24] core-shell geometry,[27] or confined supramolecular orientation.[25] Pai *et al.* demonstrated improvements in tensile modulus and strength of individual polyamide fibers with decreasing diameter, and correlated these improvements with higher molecular orientation, as measured by polarized FTIR spectroscopy.[22] They explained the improved molecular orientation to be the result of higher extension and faster solidification of the smaller diameter fibers. Greenfeld *et al*. subsequently proposed a model to relate the increased modulus to extensional flow of an entangled solution via the flow-induced molecular orientation.[28] Among the highest performing nanofibers, Dzenis and co-workers reported 250 nm diameter electrospun polyacrylonitrile fibers having Young's modulus, strength, and toughness values as high as 48 GPa, 1.75 GPa, and 0.6 GPa, respectively.[29] Yao *et al.* reported 2.1 μm diameter electrospun *p*-aramid fibers with a Young's modulus of 59 GPa,[30] and co-polyimide fiber bundles with a Young's modulus of 38 GPa and strength of 1.6 GPa.[31] To our knowledge, the highest reported Young's modulus of an electrospun fiber thus far was achieved by Boland and co-workers, who reported single-walled carbon nanotube/polyvinyl alcohol composite fibers with Young's moduli up to 85 GPa.[32] Despite such recent efforts to fabricate ultrafine high performance fibers, electrospun fibers still fall significantly short of the state of the art in high performance fibers.[33]

Because of its linear zig-zag conformation and small molecular cross-section, crystalline polyethylene has one of the highest theoretical values of Young's modulus for a polymer. [34]

High performance polyethylene fibers (e.g. Spectra or Dyneema) are fabricated using a process called "gel-spinning", wherein gel-like fibers are formed from a polymer solution comprising as little as 2 wt% of high molecular weight polymer.[35,36] Subsequently, the gel-like fibers are drawn 40 to 50 times their original length at elevated temperature, using strain rates around 1 s^{-1}. Such high drawability is made possible by the ultra high molecular weight polyethylene used (UHMWPE, typically 3000 kg mol^{-1} or more), and results in a very high level of molecular orientation and crystallinity. This commercial process leads routinely to fibers with tensile moduli (E) of 120-170 GPa and tensile strengths (σ) of 3.0-3.5 GPa.[35,36] Post-spin drawing of the gel-like fiber has been described as essential to the realization of high modulus and strength in flexible chain polymers like PE.[37]

There have been several efforts in the past to electrospin PE melt[38], LLDPE[39], HDPE[40] and UHMWPE[41], with one study attempting to control the ambient temperature during spinning with a coaxial stream of heated vapor.[42] Despite such efforts, all of them [38-42] faced difficulties in achieving thin, monodisperse PE fibers with high mechanical properties. In general, electrospinning of PE is complicated by its poor solubility in polar solvents commonly used for electrospinning, and the necessity to elevate and control process temperatures. Most of the previous efforts resulted in fabrication of fiber diameters larger than a micron, and none of them reported noteworthy mechanical properties for the fibers. Post-spin drawing such as that employed in gel-spun PE fibers is normally precluded for electrospun fibers since they are not readily spooled and re-processed as continuous fibers; as a result, efforts to improve fiber mechanical properties of electrospun PE by post-processing has been limited. Using a micromanipulator, Li *et al.*, produced single UHMWPE nanofibers with diameters on the order

of 100 nm.[43] In their two-stage process, a droplet of UHMWPE gel was heated to 120 °C, while the surrounding space was heated to 90 °C, and then drawn into a filament using the micromanipulator tip. These nanofibers reportedly exhibited tensile moduli comparable to or exceeding the theoretical value of 280 GPa. However, the hot tip-drawing process is tedious and does not lend itself well to scale-up.

In this work, we report fabrication of ultrafine, high performance PE fibers using a technique dubbed "gel-electrospinning". Unlike other elevated temperature electrospinning methods, the proposed process operates within a range of process temperatures chosen to induce the formation of a gel filament "in flight", which is drawn by the whipping motion of the jet. The modified electrospinning process, in principle, operates at a higher extensional strain rate (~1000 s^{-1}) than that of the gel-spinning process (~1 s^{-1}), and results in significantly smaller diameter fibers. Importantly, the smallest fibers exhibit remarkable mechanical properties and can be produced in quantity.

Materials and Methods

Masterials: Ultra-high molecular weight polyethylene (UHMWPE) with an intrinsic viscosity of 2100 cm^3 g^{-1} was purchased from Celanese (Irving, TX). Using Margolies' equation, the molecular weight corresponds to 4500 kg mol^{-1}, according to the vendor. *p*-Xylene, cyclohexanone, decalin, and tetra-n-butylammonium bromide (TBAB) were all purchased from Sigma-Aldrich. The solution components were combined on a heated (~120 $^{\circ}$C) stirrer for at least 2 hours.

Solvent Selection and Preliminary Electrospinning: Since the viscoelasticity of a polymer solution depends on the choice of solvent, polymer concentration, molecular weight of the polymer, and temperature, we first examined commonly used solvents (decalin, *p*-xylene, 1:1 v/v mixture of *p*-xylene:cyclohexanone) for one that demonstrated reasonable electrospinnability for a 1 wt% solution of UHMWPE and produced small diameter fibers (see Supplementary Information S1). In each case, 0.2 wt% of TBAB was added to increase the electrical conductivity of the solution to approximately 0.2 μS cm^{-1}; the addition of this salt both improved electrospinnability and reduced fiber diameter. For these preliminary experiments, temperatures T_1 and T_2, in the solution reservoir and at the extruder exit, respectively (see Figure 1a) were both held constant at 130 °C, which was above the melting point T_m of the polymer and below the boiling point T_b of all the solvents used. Temperatures T_3 and T_4, in the draw zone and at the collector, respectively, were fixed at a room temperature. The UHMWPE/*p*-xylene solution exhibited the highest production rate and smallest fiber diameters; all subsequent experiments were performed with this solution.

Solution Characterization: The crystallization and melting temperatures of the polymer in solution were obtained by differential scanning calorimetry (DSC) (Discovery, TA Instruments). The solution was cooled from 130 °C to 40 °C, and then reheated back up to 130 °C. The heating and cooling rates were 1 $^{\circ}C\ min^{-1}$. A rheometer (AR-2000, TA Instruments) with cone-plate geometry was used to measure the viscosity of the polymer solution as a function of temperature. To prevent the loss of the volatile *p*-xylene solvent during rheometry at elevated temperature (T > 100 °C), a solvent trap filled with *p*-xylene was used. Temperature sweep experiments from 130 °C to 40 °C with a fixed oscillation frequency of 1 rad s^{-1} were performed

under two different conditions – an oscillatory stress with σ_{max} = 0.88 Pa and an oscillatory strain with γ_{max} = 0.05; these values were chosen to ensure that all measurements were made within the region of linear viscoelastic response of the solution.

Fiber Formation: A spinning solution comprising UHMWPE (1 wt%), *p*-xylene, and TBAB (0.2 wt%) was used. After mixing, the solution was transferred to a pre-heated glass syringe (Cadence Science, 20 mL). A band heater (Plastic Processing Equipment, Macedonia, OH) was used to heat the solution-filled syringe. A Macor® ceramic encasing was used as an electrical insulator between the heater and the needle, while still providing good thermal conductivity at temperatures up to 170 °C. A cylindrical ceramic space heater (Omega Engineering, Stamford, CT) was used to heat the space around the needle. The temperatures of the four process zones (Figure 1a) were T_1 = T_2 = 130 °C, while T_3 and T_4 were varied from 20 °C to 130 °C. The volumetric flow rate of the feed solution was controlled by a syringe pump (Harvard Apparatus, Holliston, MA) in the range 0.02 to 0.2 ml min^{-1}. A positive potential of +15 to +20 kV was applied to the needle, while a negative potential of -10 to -15 kV was applied to the collector, using two voltage generators (Gamma High Voltage Research, Ormond Beach, FL). The distance from the tip of the needle to the collector was 150 - 200 mm.

Fiber Characterization: A JEOL 6010LA scanning electron microscope (SEM) was used to examine the morphology of mats and bundles, and to measure fiber diameters. Prior to sample loading, the electrospun fibers were sputter-coated with gold for 30 seconds. The mean fiber diameter of at least 50 fibers were measured using ImageJ software. A Tecnai T-12 transmission electron microscope (TEM) was used to examine individual fibers of different diameter. The

UHMWPE fibers were placed on a standard copper grid, and subsequently observed under the TEM. In-situ selective area electron diffraction (SAED) was performed on individual fibers to determine their crystallite orientations. At least 10 individual samples each from groups of microfibers (d >1 μm) and submicron fibers ($d \leq 1$ μm) were observed.

The degree of crystallinity was measured using a TA Instruments Discovery Differential Scanning Calorimeter (DSC). The degree of crystallinity was obtained using $X_{DSC} = (\Delta H_m - \Delta H_c)/\Delta H_m^0$, where the specific enthalpy of fusion ΔH_m^0=293.6 J g^{-1} for polyethylene,[44] the enthalpy of cold crystallization ΔH_c= 0 (in this work), and $\Delta H_m$was obtained by integrating the melting peak from the heating scan of DSC.

A Bruker D8 with General Area Detector Diffraction System was used to measure the Wide-Angle X-ray Diffraction (WAXD) trace of fiber mats and bundles. Two-dimensional X-ray diffraction patterns were measured and integrated, after background subtraction, to obtain one-dimensional XRD patterns over the range 15.0° ≤ 2θ ≤ 60.0°. The degree of crystallinity was obtained using $I_{WAXD} = I_{xtal}/(I_{xtal} + I_{amorph})$, where I_{xtal} is the total integrated area of the crystalline peaks and I_{amorph} is the integrated area of the amorphous peak. In the case of polyethylene, the crystalline peaks for the (110) and (200) planes were found at 2θ = 21.4° and 23.9°, respectively. The amorphous halo was defined as a broad peak in the range 15.0° ≤ 2θ ≤ 25.0°. The Hermans parameter for crystallite orientation was estimated from the full-width at half maximum of the azimuthal intensity distribution of the (110) diffraction peak ($FWMH_{110}$) for a bundle of aligned fibers, assuming cylindrical symmetry with respect to the bundle axis and that the intensity was Gaussian-distributed (see Supplementary Information S2).

The mechanical properties of individual fibers were measured using a U9815A T150 Universal Testing Machine ("Nano-UTM", Agilent Technologies, Santa Clara, CA). The sample preparation and test method were described previously by Pai *et al*.[22] The method was validated using conventional gel-spun polyethylene fibers (Dyneema SK99). See Supplementary Information S3, S4 and S5 for further details of the method and validation. The force was measured as a function of the extensional strain for individual electrospun fibers in uniaxial tension at a strain rate of 10^{-3} s^{-1}. The Young's modulus was determined by linear regression of the stress-strain curve from the origin to a low strain of 0.01 mm mm^{-1}. The yield point was determined by Coplan's construction, which is also known as the "tangents technique".[45] All measurements were strained up to at least a strain of 0.2 mm mm^{-1}, while some of the samples were strained until fractured. After mechanical testing, the undeformed section of the fiber was observed under SEM to determine its diameter. The diameters of five different sections were measured to determine the mean and standard deviation of the fiber diameter. If the standard deviation of the five measurements for an individual fiber was greater than 15%, the data point was discarded.

Results

Characterization of Gel-Electrospinning Process

We divide the gel-electrospinning process into four zones: the solution reservoir, the extruder exit, the draw zone (which includes both steady jet and whipping regions), and the collector. Figure 1a shows an apparatus for the gel-electrospinning of UHMWPE. In each zone the temperature was chosen judiciously based on knowledge of the polymer solution rheology. The temperatures of the zones are labelled T_1 through T_4 in Figure 1a. For maximum gel-drawing in

the whipping zone (T_3 of Figure 1a), the temperature of the polymer solution was controlled so that it should pass through the semi-dilute gel-state, analogous to the heated drawing stage of the conventional PE gel-spinning process.[35] To determine the proper operating temperature for the extruder exit and draw zones, the solution rheology of UHMWPE in *p*-xylene was measured by oscillatory shear rheometry to determine the temperature dependence of viscosity and the gelation temperature, T_{gel}.

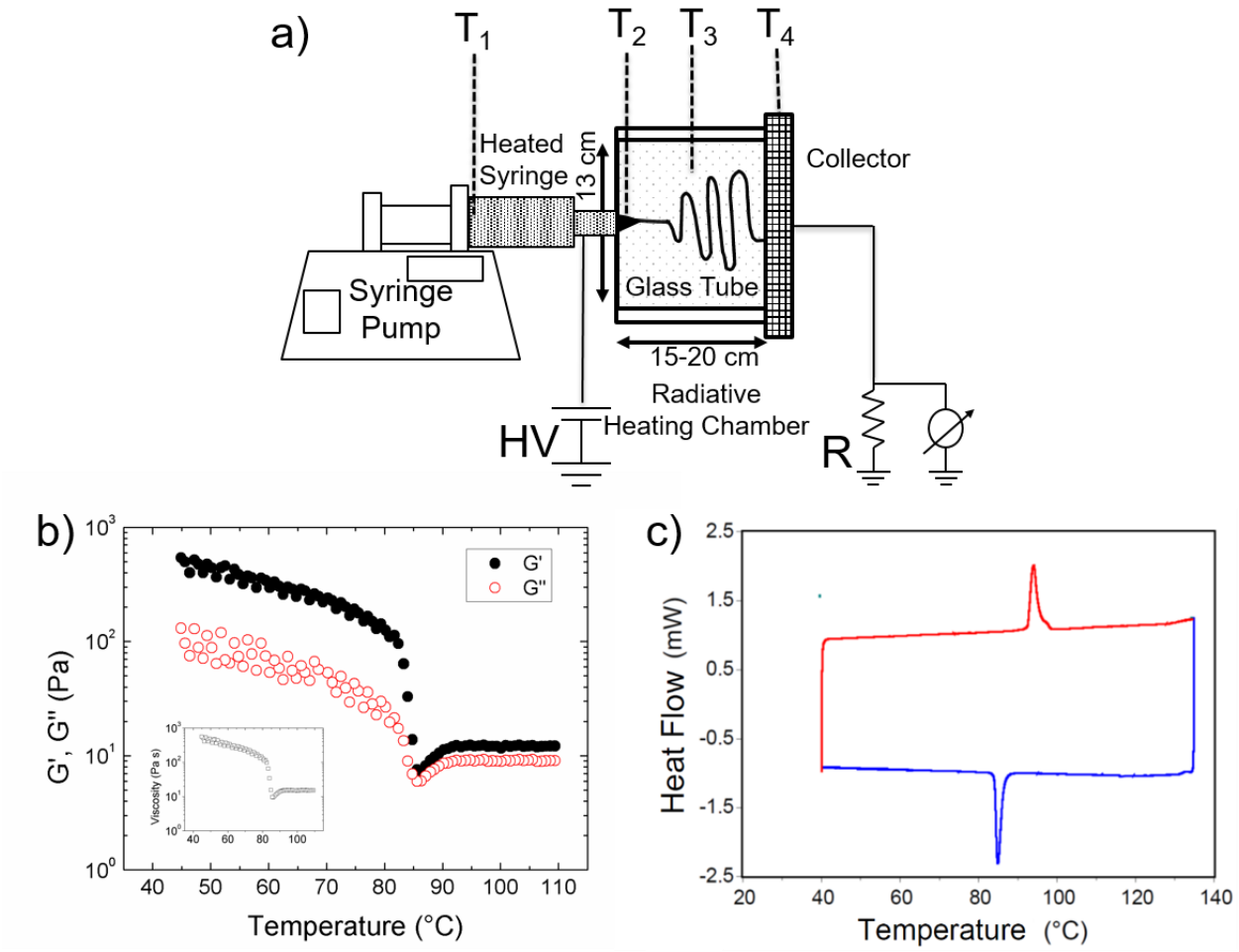

Figure 1. a) Apparatus for gel-electrospinning. T_1 = Solution reservoir temperature, T_2 = extruded jet temperature, T_3 = draw zone temperature, and T_4 = collector temperature. b) Oscillatory shear data showing the storage and loss modulus with respect to temperature under

an oscillatory stress with σ_{max} = 0.88 Pa. Filled circles represent G' and open circles represent G". The inset plots show the complex dynamic viscosities (open squares) with respect to temperature. c) Differential Scanning Calorimeter (DSC) data of UHMWPE/*p*-xylene 1 wt% solution.

Figure 1b shows the complex viscoelastic behavior of a 1 wt% UHMWPE/*p*-xylene solution under an oscillatory stress with σ_{max} = 0.88 Pa. Upon cooling, the solution viscosity was η < 20 Pa·s for T > 90 °C, and η > 100 Pa·s for T < 80 °C, with a transition in both storage (G') and loss (G") moduli between 84.7 and 81.7°C, corresponding to the gel transition. This transition was also confirmed by DSC (Figure 1c), where the onset temperature of the exotherm during the cooling cycle was 84.1 °C. Typically, a viscosity of 100 Pa·s or lower is considered suitable for continuous fiber spinning.[46] Based on these findings, the desired temperature within the draw zone for gel-electrospinning was determined to be 80 °C ≤ T_3 ≤ 85 °C, while T_1 > 90 °C. Unless stated otherwise, subsequent experiments were performed with all parameters except T_3 and T_4 held constant at these values.

Fiber Structure Characterization

Figure 2a shows the mean diameter and standard deviation for gel-electrospun fibers produced at various values of T_3. The mean fiber diameter decreased steadily as T_3 was increased from room temperature to 80 °C; above 80 °C, the mean and standard deviation of fiber diameter distribution were relatively insensitive to T_3. The decrease in fiber diameter is attributed to the decrease in elastic modulus G' over this range of temperature. Although the elastic modulus decreased by an order of magnitude above T_3 = 80 °C (*c.f.* Figure 1b), the loss modulus G" also

decreased, indicative of faster relaxation of the polymer network in solution. The UHMWPE fibers that were collected at T_3 = 80 °C showed the smallest mean fiber diameter and the narrowest fiber diameter distribution. The SEM images of representative UHMWPE fiber mats fabricated below and above T_{gel}, at T_3 = 80 °C and 120 °C, are displayed in Figure 2b. Generally, the gel-electrospun fibers, electrospun with $T_3 < T_{gel}$, exhibited smaller mean fiber diameter, albeit with a wider fiber size distribution, than the fibers produced at $T_3 > T_{gel}$. The difference in fiber sizes is evident from a comparison of the smallest individual fiber diameters observed by TEM for samples produced at 80 °C or 120 ° C, shown in Figure 2c and d. The smallest fiber shown in Figure 2c is 25 nm, comparable to the core size of a polyethylene shish-kebab structure.[47]

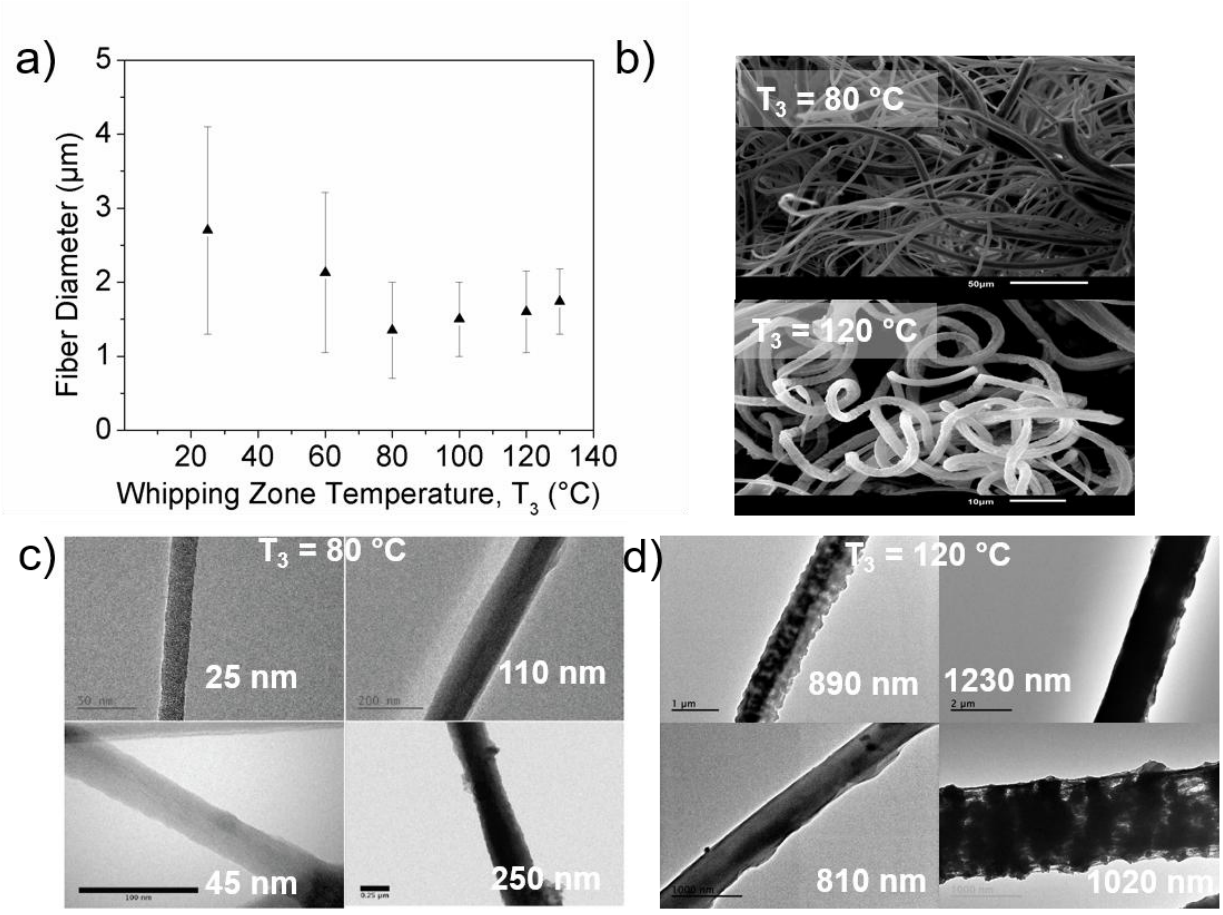

Figure 2. a) Mean diameter (filled triangles) and standard deviation for gel-electrospun UHMWPE fibers obtained using various temperatures T_3 in the drawing zone. b) SEM images of UHMWPE fiber mats fabricated at T_3 = 80 °C (below T_{gel}) and 120 °C (above T_{gel}). c,d) TEM images of individual gel-electrospun UHMWPE fibers fabricated at c) T_3 = 80 °C and d) T_3 = 120 °C. The scale bars in c) are 50 nm, 200 nm, 100 nm, and 250 nm, in clockwise order from the top left image. The scale bars in d) are 1 μm, 2 μm, 1 μm, and 1 μm, in clockwise order from the top left image.

The crystallinity of the gel-electrospun fibers was examined by DSC, WAXD and SAED. The degree of crystallinity of an UHMWPE fiber mat with $\langle d \rangle$ = 1.96 ± 0.54 μm (obtained at T_3= 60 °C) was measured by WAXD (see Supplementary Information S2) and confirmed by DSC (see Supplementary Information S6), which yielded values of 58% and 56% crystallinity, respectively. A bundle with a larger average fiber diameter, $\langle d \rangle$ = 2.35 ± 1.08 μm (obtained at T_3= 25 °C) exhibited 60% crystallinity by WAXD. By contrast, the degree of crystallinity of a sample of submicron fibers, $\langle d \rangle$ = 0.86 ± 0.39 μm (obtained at T_3= 80 °C) was close to 90%, as determined by WAXD. The crystal form was confirmed to be orthorhombic based on peak locations. The crystallite orientation, as described by the Hermans orientation parameter for the (110) plane, $\langle P_2 \rangle_{110}$, was also significantly higher for the bundle with mean fiber diameter less than 1 μm (Figure 3a). Figure 3c shows representative SAED patterns and the corresponding TEMs of individual gel-electrospun UHMWPE fibers (T_3= 80 °C) having different diameters. All of the patterns in Figure 3b are indicative of the orthorhombic PE crystal, in accord with the WAXD results. Crystal orientation within the fibers became significantly sharper with decreasing diameter. The thickest fiber with d ~ 1.95 μm (left column of Fig 3b) showed random

crystal orientation, as signified by the ring pattern in SAED; other fibers with $d > 1$ μm also displayed such patterns. The intermediate fiber with $d \sim 0.42$ μm (middle column) exhibited arc-shaped reflections, indicative of a distribution of orientations for the (110) and (200) crystal lattice planes. The highest crystal orientation was observed when $d \sim 0.11$ μm (right column), whose pattern was that typical of a single crystal. These SAED data, in general, agree with the study of individual crystal orientations in HDPE fibers by Yoshioka *et al*.[48] We conjecture that the increasing crystal orientation observed for fibers with $d \leq 1$ μm is due to the high degree of molecular alignment made possible by rapid and large extension in the gel state experienced by these fibers during whipping.

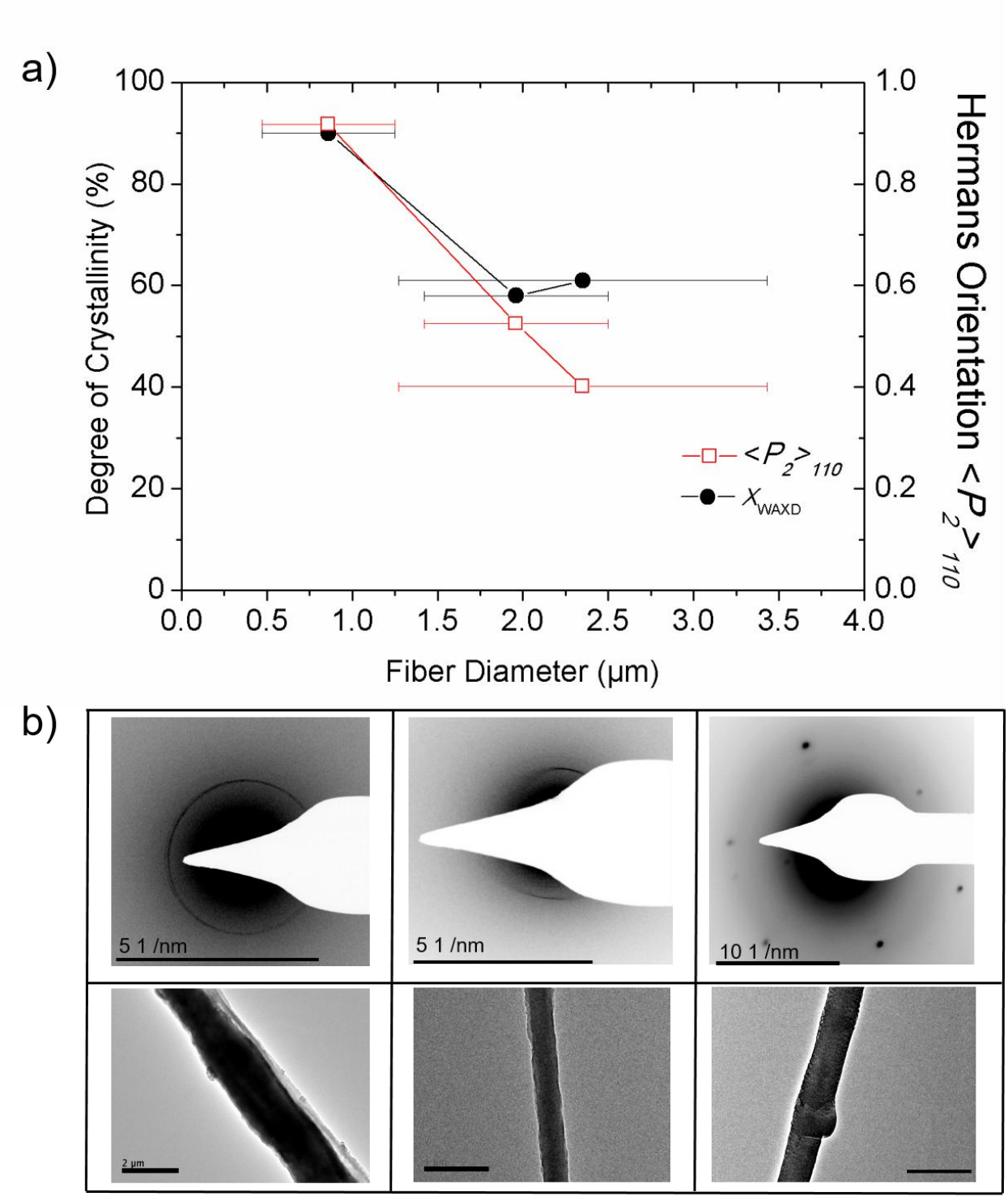

Figure 3. a) Degree of crystallinity (X_{WAXD}, left ordinate, black filled circles) and the Hermans orientation parameter ($\langle P_2 \rangle_{110}$, right ordinate, red open squares) are plotted versus average fiber diameter for three bundles of aligned fibers. Error bars correspond to standard deviation of fiber

diameter distribution measured within each bundle. b) SAED crystal patterns displayed on the top row, and the corresponding TEMs of individual UHMWPE fibers on the bottom row. The scale bars represent 2.0 μm, 1.0 μm, and 0.2 μm from the leftmost column to the rightmost column.

Mechanical Properties of Gel-Electrospun Fibers

Figure 4a shows stress-strain curves for individual gel-electrospun UHMWPE fibers with diameters of 0.49, 0.73, 0.91, 1.05, and 2.31 μm. Note that the smallest of these fibers corresponds to a crystallite orientation intermediate between the center and right columns of Figure 3b. The Young's moduli were determined from the slope of linear regression in the region of small strain, up to 0.01 mm mm^{-1}. The moduli are plotted against fiber diameter in Figure 4b; a dramatic increase in Young's modulus is observed for fibers whose diameters were less than 1 μm. Many of the submicron UHMWPE fibers exhibited Young's moduli above 30 GPa, while those fibers with $d \leq 0.60$ μm exhibited moduli above 100 GPa. In particular, the Young's modulus of a fiber with diameter 0.35 ± 0.05 μm was measured at 120 ± 24 GPa. Significantly, this value is the highest reported modulus for a single fiber produced by any electrostatically-driven jetting process, and is comparable to that of a commercial high performance fiber (i.e. Dyneema SK99, see Table 1). The mean Young's modulus of the submicron diameter fibers ($d < 1$ μm) was 73 ± 13 GPa, which is two orders of magnitude higher than the Young's modulus of bulk UHMWPE,[49] and better than the best electrospun fibers to date.

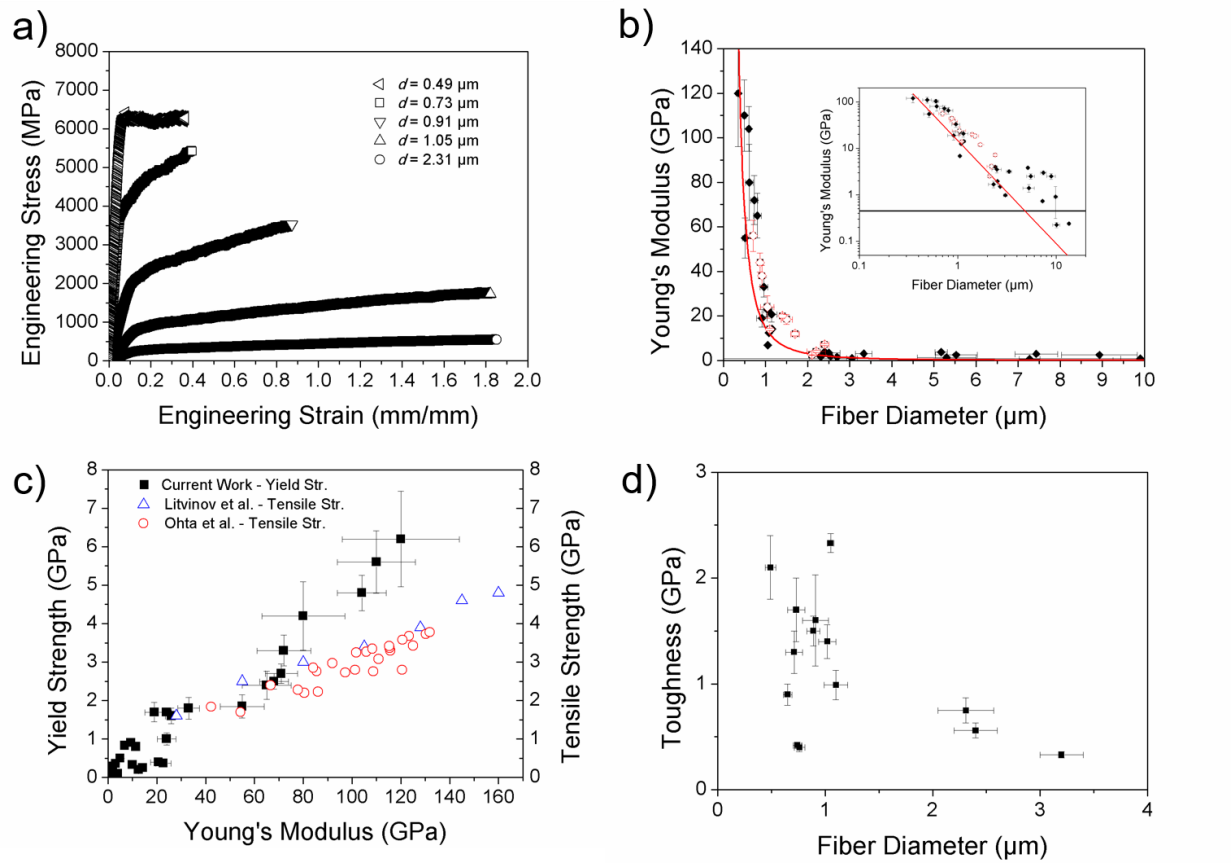

Figure 4. Tensile deformation behavior of gel-electrospun UHMWPE fibers. a) Stress-strain curves for UHMWPE fibers having diameters of 0.49 (◁), 0.73 (□), 0.91 (▽), 1.05 (△), and 2.31 μm (○). b) Young's modulus versus fiber diameter. Inset shows the same data on a log-log scale. The solid line at 0.45 GPa is the Young's modulus of bulk UHMWPE.[49] The red solid line is an empirical fit (see text for details). c) Strength versus Young's modulus of each corresponding fiber. The black squares show yield strengths measured in the current study, while the blue triangles and red circles show tensile strengths of conventional gel spun fibers reported in the literature;[50,51] since the conventional fibers exhibited brittle failure at relatively low strain, their tensile strengths are assumed to be lower bounds for yield. d) Toughness versus fiber diameter.

Table 1. Mechanical properties for gel-electrospun UHMWPE fibers averaged over a range of diameters, Dyneema SK99, and bulk UHMWPE.[49] See Supplementary Information S8 for a table of mechanical properties for individual fiber data and reproducibility.

Fiber Diameter (μm)	Hencky Strain	Young's Modulus (GPa)	Ultimate Tensile Strength (GPa)	Toughness (GPa)	Strain at Break
0.57±0.03	9.98	89±9	4.9±0.5	1.5±0.2	0.31
0.73±0.03	9.46	48±3	3.0±0.2	0.96±0.09	0.46
0.90±0.07	9.07	23±2	2.9±0.4	1.9±0.2	0.80
1.06±0.05	8.74	9.22±0.64	1.63±0.10	1.57±0.07	1.13
2.64±0.13	6.92	5.56±0.37	0.72±0.05	0.55±0.14	1.26
12.2±0.5 (Dyneema SK99)	--	131±8	4.18±0.24	0.145±0.008	0.05
Bulk UHMWPE	0	0.72	~ 0.02	--	~ 0.50

The remarkable increases in modulus observed in the smallest fibers reported here are attributed to the large amplitude of the whipping instability, which resulted in high draw ratio, high degree of crystallinity, and high crystallite orientation. In the conventional, two-stage gel-spinning process, the properties of fibers have been found to be sensitive to the draw ratio applied in the second stage, solid-state hot-drawing of the gel filament.[35] Gel-electrospinning is a single stage process where drawing of the filament occurs "in-flight", both at the nozzle and during whipping, where the solvent content of the jet is changing; it is difficult therefor to determine exactly where in the process the gel point is reached and solid state drawing begins. However, one can estimate a Hencky strain, $\varepsilon = 2ln(h_0/h)$,[52] where h_0 is the diameter of the unstretched fluid filament at

the nozzle exit (840 μm), and h is the diameter of the stretched fluid filament assuming rapid solidification, $h = d/\sqrt{c}$. d is the diameter of the solid as-spun fiber and c is the concentration of polymer in solution.[53] The data of Figure 4b are well-described by the empirical correlation $E[GPa] = 14.9(d[\mu m])^{-2.22}$, with a coefficient of determination $R^2 = 0.97$. In terms of Hencky strain, this correlation can be written as $E = Aexp(B\varepsilon)$, where A=8.65x10^{-3} GPa and B=1.11. The corresponding fiber diameters and Hencky strains are tabulated in Table 1.

Figure 4c shows the correlation between yield strength and the tensile modulus measured for the gel-electrospun fibers. Not only the modulus, but also the yield strength increased as the fiber diameter decreased, by as much as 600-fold from the largest diameter fibers to the smallest ones (see Supplementary Information S7). A similar trend, albeit much smaller in magnitude, was observed previously by Pai *et al.*[22] The mean yield strength for submicron diameter fibers (d < 1 μm) was 3.5 ± 0.6 GPa, which is two orders of magnitude higher than that of bulk UHMWPE.[49] Also shown in Figure 4c are correlations between ultimate tensile strength and tensile modulus for conventional gel-spun fibers reported in the literature.[50,51] Although the data overlap for fibers having moduli below about 70 GPa (characteristic of the larger diameter gel-electrospoun fibers), the two sets deviate at high modulus, where the yield strength of the smallest diameter gel-electrospun fibers exceed the tensile strength of the conventional fibers. The ultimate tensile strength of the UHMWPE fibers with average d = 0.57 μm was greater than the ultimate tensile strength of Dyneema SK99. The best tensile strength obtained in this work was 6.3 GPa, for a fiber with d = 0.49 μm. A composite UHMWPE/CNT fiber yarn electrospun by Rein *et al.* showed a slightly higher tensile strength of 6.6 GPa after post-spin drawing.[54]

Toughness was also observed to increase with reduction in fiber diameter (c.f. Figure 4d). Significantly, most of the fibers below 1 μm in diameter exhibited toughnesses greater than 1.0 GPa, with the highest ones exceeding 2.0 GPa. Remarkably, even at room temperature, the gel-electrospun fibers exhibited yield and ductility, with strains-to-break that were typically 20% or higher. This result stands in contrast to that of most other high performance fibers, which exhibit brittle failure at low strain.[55] Significantly, Jenket *et al.* reported increased ductility in commercial gel-spun UHMWPE fibers (Dyneema SK76) at an elevated temperature of 75 °C and low strain rate of 10^{-3} s^{-1} (comparable to the strain rate used in this work) with strains-to-break in excess of 25% (the limit of their equipment).[56] Papkov *et al.*[29] also observed a dramatic increase of toughness with decreasing fiber diameter in electrospun fibers. However, the toughnesses observed here are three times greater than the highest value reported by Papkov *et al.* and their semicrystalline PAN fibers showed lower crystallinity below d = 1 μm, so that they attributed the large elongation-to-break to ductility of the noncrystalline material.

Figure 5 shows SEM images of individual gel-electrospun UHMWPE fibers with d = 0.35 ± 0.05, 1.1 ± 0.1, and 3.2 ± 0.2 μm, before and after tensile testing. The uniformity of diameter of individual fibers prior to tensile testing is evident in Figure 5a. Figure 5b shows the same fibers after elongation to 20%, 91% and 110% strain, respectively, all without breaking. Each of the fibers exhibits reduction in diameter with elongation, on the order of 8.5%, 35% and 47%, corresponding to Poisson's ratios around 0.4 ± 0.02. In addition, the smaller fibers showed signs of necking near the middle of the test section, with 15-20% further diameter reduction. Such necking behavior is typical of ductile deformation in semicrystalline polyethylene, and is usually associated with a transition from lamellar to fibrillar texture.[57,58]

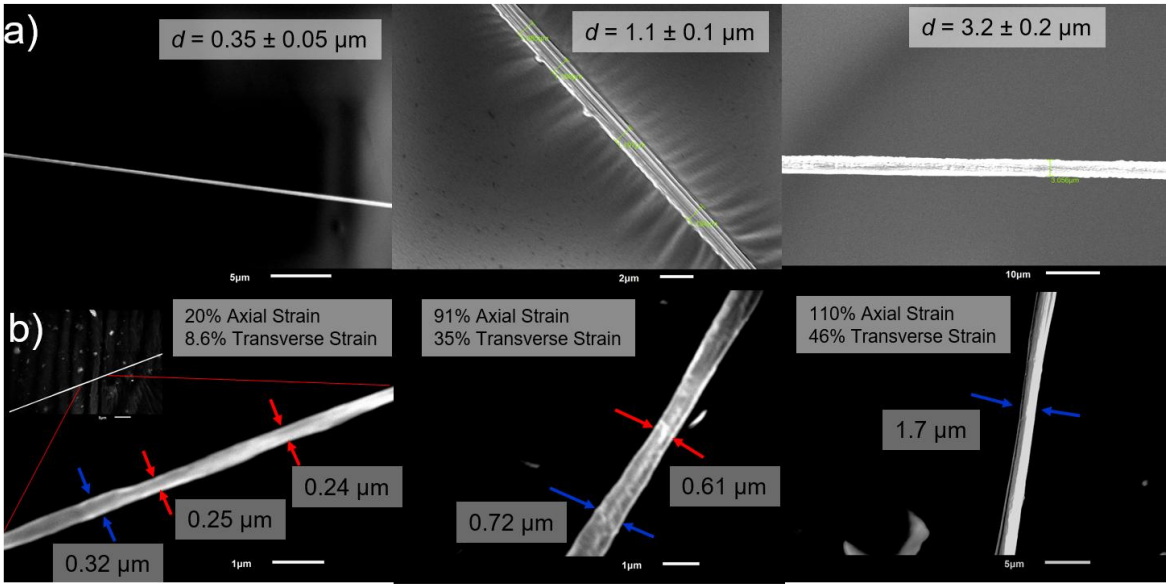

Figure 5. SEM images of individual gel-electrospun UHMWPE fibers a) before and b) after tensile deformation. The blue arrows indicate regions where diamter reduction was uniform, while the red arrows indicate regions of localized necking.

Discussion

In order to understand the origin of the improvements in strength and toughness observed in these submicron diameter fibers, these properties were first correlated using Griffith's theory of fracture,[59] according to which the tensile strength increases with a reduction in geometrical dimension, which in turn is presumed to limit crack length. Although originally developed to explain brittle fracture in linear elastic materials, the theory was subsequently applied to the development of plastic zones (e.g. crazes) followed by fracture, as well.[60] Based on this theory, Penning *et al.* derived a correlation between tensile strength σ, toughness G_c, modulus E and fiber diameter d, such that $\sigma \sim (G_c E/d)^{\alpha}$, with α = 0.5.[61] From the log-log plot of σ versus $G_c E/d$ in Figure 6, we obtain the empirical value α = 0.37, with a coefficient of determination

R^2 = 0.91. Although the correlation appears good, the value of α is significantly smaller than the theoretical value 0.5, yet it is larger than the value of α = 0.19 obtained by Penning *et al.* for conventional gel-spun polyethylene filaments having moduli of 150 GPa and diameters ranging from 8 to 30 μm.[61] Extrapolating the data in Figure 6 to d = 0 (see Supplementary Information S7), we obtain an empirical estimate for the limiting tensile strength of 14 GPa, which is intermediate between the value of 10 GPa reported by Litvinov *et al.*[50] and 26 GPa reported by Smook *et al.*[62] Due to the smaller fiber diameters obtained, the extrapolation required in this work is relatively modest compared to the previous studies.

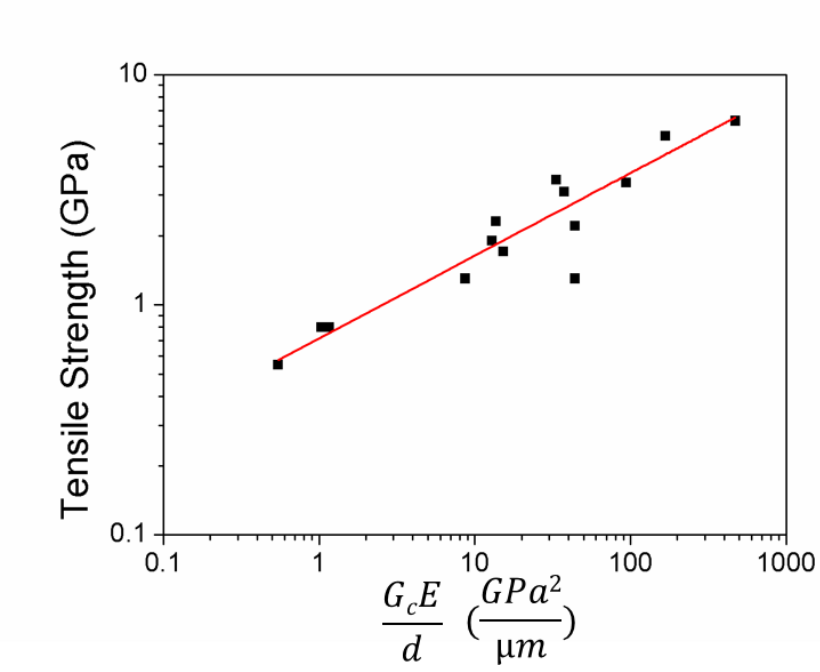

Figure 6. A log-log plot of tensile strength versus the quantity ($G_c E/d$) where G_c = fracture toughness [GPa], E = elastic modulus [GPa], and d = fiber diameter [μm]. The red solid line is an empirical fit (see text for details).

The combinations of tensile modulus, tensile strength and toughness observed at room temperature in this work merit further comment. The theoretical limit of stiffness for a perfectly oriented, fully crystalline PE is about 280 GPa at 300 K[33], and values greater than 150 GPa have been reported for gel-spun fibers.[63] Tensile moduli depend predominantly on degree of crystallinity and crystallite orientation. Theoretical values for chain slip in crystalline PE are on the order of 6-8 GPa[64] comparable to the best values of yield strength observed here. Yield strength greater than 6 GPa has also been reported for conventional gel-spun PE fibers, where it was shown to be a function of crystallite size and orientation.[63] The theoretical value for Poisson's ratio of the orthorhombic crystal of polyethylene is about 0.4 at 300 K[34], in accord with those estimated from SEM images in Figure 5. Theoretical estimates of the ultimate tensile strength associated with chain scission are around 20-25 GPa[64], somewhat higher than the limiting tensile strength obtained here by extrapolation of the Griffith criterion. Thus, the values of stiffness and strength observed for gel-electrospun fibers are well within theoretical and previous experimental bounds.

As we show with WAXD and SAED (*c.f.* Figure 3), smaller diameter fibers exhibit higher crystallinity and better crystallite orientation, which accounts for the dominant trend of increasing modulus and strength with decreasing fiber diameter. Often, crystallite size and degree of crystallinity are correlated in materials produced by a given process (e.g. gel-spinning), so that similar correlations in strength and stiffness may be expected, as illustrated in Figure 4c; however, it is not necessarily the case when comparing materials produced by different processes. For example, Bastiaansen examined gel-spun UHMWPE fibers produced from solutions having different concentrations and drawn to varying extents, and observed essentially no dependence of tensile strength on fiber diameter in the range from 20 to 250 μm,[65] while

more recently, Ohta *et al.* reported remarkably good correlation of σ_f with $(E/d)^{1/2}$ for fibers produced at different spinning speeds.[51] These discrepancies are presumably due to differences in internal morphologies of the fibers examined in the different studies. Using solid state NMR in conjunction with WAXD and SAXS, Litvinov *et al.* observed chain-extended crystals and nanovoids in conventional gel-spun fibers.[50] Using FIB and AFM, Strawhecker *et al.* examined the interior morphology of single fibers of Spectra and Dyneema, and found inter-locked shish-kebabs, voids, and defects.[66] Some of the larger gel-electrospun fibers observed in this work also exhibited some evidence of shish-kebab morphologies in TEM, regardless of draw zone temperature (*c.f.* Figure 2d). These structural defects could explain the lower tensile strength observed with conventional gel-spun polyethylene microfibers relative to theoretical values.[62] By contrast, the submicron diameter polyethylene fibers reported in this work exhibit yield strengths remarkably close to theoretical values for chain slip within the orthorhombic crystal, suggesting that smaller diameter reduces the likelihood of premature failure due to such defects and allows sustained loads sufficient to activate the slip mechanism at the yield point.

With the mechanism of chain slip in mind, we postulate that the relatively high surface area of the ultrafine gel-electrospun UHMWPE fibers is responsible for the high elongation-to-break. Given the increases observed in crystallinity and crystallite orientation with decreasing fiber diameter, it seems unlikely that such high elongation-to-break can be attributed solely to the ductility of noncrystalline material in the smallest fibers. In highly oriented fibers such as the ones produced by gel-electrospinning, yield and failure are believed to occur through molecular processes of chain slip and chain scission within the chain extended crystal.[67] Based on the theoretical values, chain scission occurs at stresses only 3-4 times greater than the stress required

to activate chain slip. Thus, as the yield stress is approached, any local concentration of stress could lead to chain scission, followed by a cascade of subsequent chain scission events, resulting ultimately in failure. In submicron diameter fibers, however, chain slip at the surface of the fiber becomes significant. In a fiber having d = 500 nm, almost 10% of the chains are within 10 nm of the fiber surface; such chains experience weaker inter-chain interactions, even within a chain extended crystal, due to their proximity to a surface. As a result, they may undergo slip more readily, permitting a degree of molecular mobility associated with the crystalline domains analogous to that produced by elevated temperatures in conventional gel-spun UHMWPE fibers elongated at comparable rates.[56] Ability of chain slip to dissipate stress concentrations and delay the initiation of a chain scission cascade would account for the substantial ductility observed in conventional gel-spun fibers at high temperature, as well as the submicron diameter gel-electrospun fibers reported here. The chain slip mechanism is also qualitatively consistent with the observed necking in Figure 5, indicative of transition from "slip-free" to "slip-activated" material.

The combinations of stiffness, strength, and elongation-to-break observed here may be unique among polymer fibers, but are not without precedent in other materials. Such combinations of properties are found in metal nanowires,[68] which are also very different from their more macroscopic counterparts. There too, it is believed that such material properties are due to the combination of fewer defects and greater contributions from surface atom interactions with reduction of diameter.[68] Notably, a gold nanowire was reported to exhibit a true strength of 6-9 GPa with elongation-at-break as high as 26% in a tensile test.[69] The high ductility observed there also involved formation of a neck, which persisted up to a high strain until break. Similarly

a nickel nanowire exhibited unusually high shear strain-to-break of 34%,[70] comparable to the high strain-to-break observed in the current study.

Conclusion

In this work, we present evidence for a new class of high performance polymer fibers with exceptional stiffness, strength and toughness. The fibers are noteworthy for their small diameter and corresponding high specific surface area. The fibers are fabricated from UHMWPE by a process called "gel-electrospinning", wherein the drawing of an entangled polymer gel at elevated temperature is realized in the whipping zone. Figure 7 compares the mechanical properties observed in this study with those of various high-performance commercial fibers. In general, high performance fibers exhibit moduli well above 100 GPa and tensile strengths greater than 2.0 GPa, but elongation-to-break generally around 3-4%, with correspondingly low toughness by comparison. The gel-electrospun UHMWPE fibers, in general, show increases in modulus and strength as the fiber diameter is decreased, with the smallest fibers exhibiting moduli in the high performance range, and strengths greater even than that of Zylon® (PBO) fiber.[52] Even with such high strength and modulus, elongation-to-break on the order of 20-40% was observed in the smallest fibers. In particular, fiber with a diameter of 490 ± 50 nm showed a Young's modulus of 110 ± 16 GPa, ultimate tensile strength of 6.3 ± 0.9 GPa, and toughness of 2.1 ± 0.3 GPa, which is a combination of mechanical properties that is unparalleled among submicron diameter polymer fibers to date. With a toughness of about 0.165±0.030 GPa, spider dragline silk is often noted for its superior toughness and extensibility compared to synthetic fibers[71], but this is only a fraction of the toughness exhibited by the smallest fibers reported here. We believe this work represents an important step towards production of thinner, high performance fibers for composites, protective clothing and other applications.

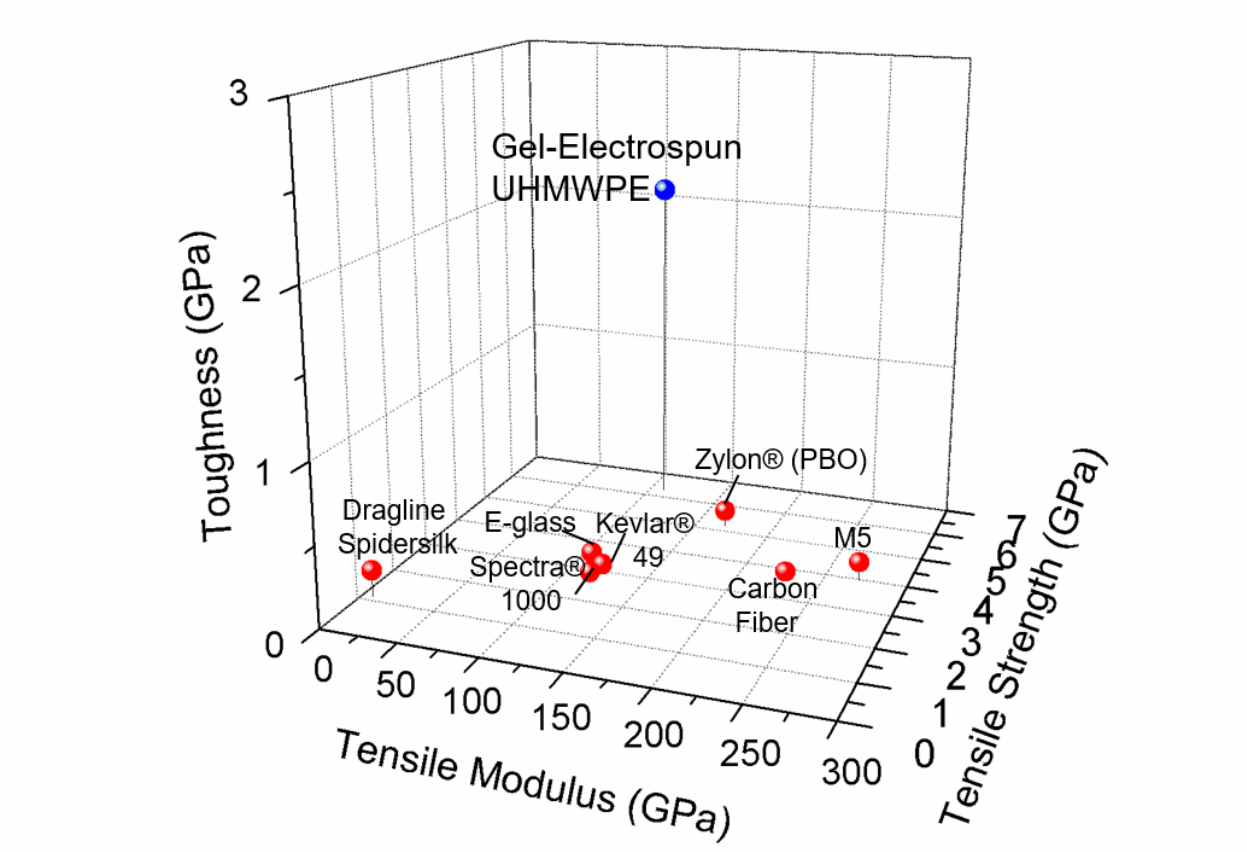

Figure 7. Three-dimensional plot of tensile modulus, tensile strength, and toughness for the individual gel-electrospun UHMWPE fibers with different diameters, several commercial polymer fibers[55], and spider dragline silk[71]

Supplementary Information.

S1: Results using different solvents. S2: WAXD data. S3: Detailed description of individual fiber mechanical test. S4: Testing for a possible clamp slippage. S5: Validation of mechanical testing usig Dyneema SK99. S6: DSC data. S7: Yield strength vs diameter and limiting tensile strength. S8: Results of individual fiber tests and reproducibility.

Corresponding Author

Gregory C. Rutledge* rutledge@mit.edu*

ACKNOWLEDGMENT

Funding for this work was provided by the U.S. Army through the Natick Soldier Research, Development and Engineering Center (NSRDEC). The authors are grateful to the U.S. Army-funded Institute for Soldier Nanotechnologies (ISN) and the National Science Foundation-funded Center for Materials Science and Engineering (CMSE) for use of facilities and equipment. This work made use of the MRSEC Shared Experimental Facilities at MIT, supported by the National Science Foundation under award number DMR-14-19807.

REFERENCES

[1] Shin YM, Hohman MM, Brenner MP, Rutledge, GC (2001) Electrospinning: A Whipping Fluid Jet Generates Submicron Polymer Fibers. Appl. Phys. Lett. 78:1149-1151.

[2] Reneker DH, Yarin AL, Fong H, Koombhongse S. (2000) Bending Instability of Electrically Charged Liquid Jets of Polymer Solutions in Electrospinning. J. Appl. Phys. 87:4531-4547.

[3] Liu C, Hsu P-C, Lee HW et al (2015) Transparent Air Filter For High-Efficiency PM2.5 Capture. Nat. Comm. 6: 6205-6205-9.

[4] Gopa R, Kaur S, Ma Z, Chan C, Ramakrishna S, Matsuura T (2006) Electrospun Nanofibrous Filtration Membrane. J. Membr. Sci. 281:581-586.

[5] Chattopadhyay S, Hatton TA, Rutledge GC (2016) Aerosol Filtration Using Electrospun Cellulose Acetate Fibers. *J. Mater. Sci.* 51:204-217.

[6] Choong LT, Khan Z, Rutledge GC (2014) Permeability of Electrospun Fiber Mats Under Hydraulic Flow. J. Membr. Sci. 451:111-116.

[7] Wang L, Yu Y, Chyen PC, Zhang DW, Chen CH (2008) Electrospinning Synthesis of C/Fe 3 O 4 Composite Nanofibers and Their Application for High Performance Lithium-ion Batteries. J. Power Sources 183:717-723.

[8] Kim C, Yang S, Kojima M, Yoshida K, Kim YJ, Kim YA, Endo M (2006) Fabrication of Electrospinning- Derived Carbon Nanofiber Webs for the Anode Material of Lithium- Ion Secondary Batteries. Adv. Func. Mater. 16:2393-2397.

[9] Kim YS, Shoorideh G, Zhmayev Y, Lee J, Li Z, Patel B, Chakrapani S, Park JH, Lee S, Joo YL (2015) The Critical Contribution of Unzipped Graphene Nanoribbons to Scalable Silicon–Carbon Fiber Anodes in Rechargeable Li-ion Batteries. 16:446-457.

[10] Wang X, Drew C, Lee SH, Senecal KJ, Kumar J, Samuelson LA (2002) Electrospun Nanofibrous Membranes for Highly Sensitive Optical Sensors. Nano Letters 2:1273-1275.

[11] Ding B, Wang M, Wang X, Yu J, Sun G. (2010) Electrospun Nanomaterials for Ultrasensitive Sensors. Mater. Today 13:16-27.

[12] Park JH, Joo YL (2014) Tailoring Nanorod Alignment in a Polymer Matrix by Elongational Flow under Confinement: Simulation, Experiments, and Surface Enhanced Raman Scattering Application. Soft Matter 10:3494-3505**.**

[13] Mo X, Xu CY, Kotaki M, Ramakrishna S (2004) Electrospun P (LLA-CL) Nanofiber: A Biomimetic Extracellular Matrix for Smooth Muscle Cell and Endothelial Cell Proliferation. Biomaterials 25:1883-1890.

[14] Zhang Y, Venugopal JR, El-Turki A, Ramakrishna S, Su B, Lim CT (2008) Electrospun Biomimetic Nanocomposite Nanofibers of Hydroxyapatite/Chitosan for Bone Tissue Engineering. Biomaterials 29:4314-4322.

[15] Pham QP, Sharma U, Mikos AG (2006) Electrospinning of Polymeric Nanofibers for Tissue Engineering Applications: A Review. Tissue Eng. 12:1197-1121.

[16] Liu W, Thomopoulos S, Xia Y (2012) Electrospun Nanofibers for Regenerative Medicine. *Adv. Healthcare Mater*. 1:10-25.

[17] Sill TJ, von Recum HA (2008) Electrospinning: Applications in Drug Delivery and Tissue Engineering. Biomaterials 29:1989-2006.

[18] Chew SY, Hufnagel TC, Lim CT, Leong KW (2006) Mechanical Properties of Single Electrospun Drug-encapsulated Nanofibres. Nanotechnology 17:3880-3891.

[19] Wong SC, Baji, A, Leng S. (2008) Effect of fiber diameter on tensile properties of electrospun poly (ε-caprolactone). Polymer 49:4713-4722.

[20] Naraghi M, Chasiotis I, Kahn H, Wen Y, Dzenis Y. (2007) Novel Method for Mechanical Characterization of Polymeric Nanofibers. Rev. Sci. Instrum. 78:085108.

[21] Finn N (2013) Types of Smart Materials for Protection in *Smart Textiles for Protection* Woodhead Publishing, Cambridge.

[22] Pai CL, Boyce MC, Rutledge GC (2011) Mechanical Properties of Individual Electrospun PA 6 (3) T Fibers and Their Variation with Fiber Diameter. Polymer 52:2295-2301.

[23] Pai CL, Boyce MC, Rutledge GC (2011) On The Importance of Fiber Curvature to The Elastic Moduli of Electrospun Nonwoven Fiber Meshes. Polymer 52:6126-6133.

[24] Ji Y, Li B, Ge S, Sokolov JC, Rafailovich MH (2006) Structure and Nanomechanical Characterization of Electrospun PS/Clay Nanocomposite Fibers. Langmuir 22:1321-1328.

[25] Arinstein A, Burman M, Gendelman O, Zussman E (2007) Effect of Supramolecular Structure on Polymer Nanofibre Elasticity. Nat. Nanotechnol 2:59-62.

[26] Richard-Lacroix M, Pellerin C (2013) Molecular Orientation in Electrospun Fibers: from Mats to Single Fibers. Macromolecules 46:9473-9493.

[27] Reneker DH, Yarin AL, Zussman E, Xu H (2007) Electrospinning of Nanofibers from Polymer Solutions and Melts. in *Advances in Applied Mechanics*; Hassan, A., van der Erik , G., Eds. Elsevier. Amsterdam, 41:43−346.

[28] Greenfeld I, Sui XM, Wagner HD (2016) Stiffness, Strength, and Toughness of Electrospun Nanofibers: Effect of Flow-Induced Molecular Orientation. Macromolecules 49: 6518-6530.

[29] Papkov D, Zou Y, Andalib MN, Goponenko A, Cheng SZD, Dzenis YA (2013) Simultaneously Strong and Tough Ultrafine Continuous Nanofibers. ACS Nano 7:3324-3331.

[30] Yao J, Jin J, Lepore E, Pugno NM, Bastiaansen CWM, Peijs T (2015) Electrospinning of *p*-Aramid Fibers. Macro. Mater. Eng. 12:1238-1245.

[31] Yao J, Pantano MF, Pugno NM, Bastiaansen CWM, Peijs T (2015) High-Performance Electrospun Co-Polyimide Nanofibers. Polymer 76:105-112.

[32] Almecija D, Blond D, Sader JE, Coleman JN, Boland JJ (2009) Mechanical Properties of Individual Electrospun Polymer-Nanotube Composite Nanofibers. Carbon, 47:2253-2258.

[33] Park JH, Rutledge GC (2017) 50th Anniversary Perspective: Advanced Polymer Fibers: High Performance and Ultrafine, Macromolecules, 50:5627-5642.

[34] Lacks DJ, Rutledge GC (1994) Simulation of the Temperature Dependence of Mechanical Properties of Polyethylene, J. Phys. Chem. 98:1222-1231.

[35] Smith P, Lemstra PJ (1980) Ultra-High-Strength Polyethylene Filaments by Solution Spinning/Drawing. J. Mater. Sci. 15, 505-514.

[36] Smith P, Lemstra PJ (2009) Production and Properties of High-modulus and High-strength Polyethylene Fibres. in Handbook of Textile Fiber Structure, Vol 1. Eichhorn *et al.* (eds.) Ch 12 352-393.

[37] Yao J, Bastiaansen CMW, Peijs T (2014) High Strength and High Modulus Electrospun Nanofibers. Fibers 2:158–186.

[38] Larrondo L, St. John Manley R (1981) Electrostatic Fiber Spinning from Polymer Melts. I. Experimental Observations on Fiber Formation and Properties. J. Polym. Sci.-Phys. 19:909-920.

[39] Givens SR, Gardner KH, Rabolt JF, Chase DB (2007) High-Temperature Electrospinning of Polyethylene Microfibers from Solution. Macromolecules 40:608-610.

[40] Yoshioka T, Dersch R, Greiner A, Tsuji M, Schaper AK (2010) Highly Oriented Crystalline PE Nanofibrils Produced by Electric- Field- Induced Stretching of Electrospun Wet Fibers. Macromol. Mater. Eng. 295:1082-1089.

[41] Rein DM, Shavit-Hadar L, Khalfin RL, Cohen Y, Shuster K, Zussman, E (2007) Electrospinning of Ultrahigh- Molecular- Weight Polyethylene Nanofibers. J. Polym. Sci.-Phys. 45:766-773.

[42] Rein DM, Cohen Y, Ronen A, Shuster K, Zussman E. (2009) Application of Gentle Annular Gas Veil for Electrospinning of Polymer Solutions and Melts. Polym. Eng. Sci. 49:774-782.

[43] Li P, Hu L, McGaughey AJH, Shen S (2014) Crystalline Polyethylene Nanofibers with the Theoretical Limit of Young's Modulus. Adv. Mater. 26:1065-1070.

[44] CRC Handbook of Chemistry and Physics, 97th ed, CRC Press, (2016).

[45] Ward IM (1983) in *Mechanical Properties of Solid Polymers*. 2nd ed. New York, NY Wiley.

[46] Gahleitner M (2001) Melt Rheology of Polyolefins. Prog. Polym. Sci. 26:895-944.

[47] Grubb DT, Keller A (1978) Thermal Contraction and Extension in Fibrous Crystals of Polyethylene. Colloid. Polym. Sci. 256:218-233.

[48] Yoshioka T, Dersch R, Tsuji M, Schaper AK (2010) Orientation Analysis of Individual Electrospun PE Nanofibers by Transmission Electron Microscopy. Polymer 51:2383-2389.

[49] GUR® 4120; MSDS No.21003915; Ticona: Florence, KY November 02, (2010)

[50] Litvinov VM, Xu J, Melian C, Demco DE, Möller M, Simmelink J (2011) Morphology, Chain Dynamics, and Domain Sizes in Highly Drawn Gel-Spun Ultrahigh Molecular Weight

Polyethylene Fibers at the Final Stages of Drawing by SAXS, WAXS, and 1H Solid-State NMR. Macromolecules 44:9254–9266.

[51] Ohta Y, Murase H, Hashimoto T (2005) Effects of Spinning Conditions on the Mechanical Properties of Ultrahigh-Molecular-Weight Polyethylene Fibers. J. Polym. Sci. B. 43:2639–2652.

[52] McKinley GH, Sridhar T (2002) Filament-Stretching Rheometry of Complex Fluids. Annu. Rev. Fluid. Mech. 34:375-415.

[53] Fridrikh SV, Yu JH, Brenner MP, Rutledge GC (2003) Controlling the Fiber Diameter during Electrospinning. Phys. Rev. Lett. 90:144502-144502-4.

[54] Rein DM, Cohen Y, Lipp J, Zussman E (2010) Elaboration of Ultra- High Molecular Weight Polyethylene/Carbon Nanotubes Electrospun Composite Fibers. Macromol. Mater. Eng. 295, 1003-1008.

[55] Chae HG, Kumar S (2006) Rigid-rod Polymeric Fibers. J. App. Poly. Sci. 100:791–802.

[56] Jenket DR, Forster AM, Paulter NG, Weerasooriya T, Gunnarsson CA, Al-Sheikhly M (2017) An Investigation of the Temperature and Strain-Rate Effects on Strain-to-Failure of UHMWPE Fibers. in Challenges in Mechanics of Time-Dependent Materials, Vol 2, B. Antoun et al (eds.), Ch 4, 23-33.

[57] Peterlin A (1971) Molecular model of drawing polyethylene and polypropylene. J. Mater. Sci. 6:490-508.

[58] Jiang Z, Tang Y, Rieger, J, et al (2009) Structural evolution of tensile deformed high-density polyethylene at elevated temperatures: Scanning synchrotron small- and wide-angle X-ray scattering studies. Polymer 50:4101-4111.

[59] Griffith AA (1921) The Phenomena of Rupture and Flow in Solids. Philos. Trans. R. Soc. A 221:163–198.

[60] Williams JR (1978) Applications of Linear Fracture Mechanics Adv. Polym. Sci. 27:69-120.

[61] Penning JP, De Vries AA, Van der Ven J, Pennings AJ, Hoogstraten, HW (1994) A Study of Transverse and Longitudinal Size Effects in High-Strength Polyethylene Fibres. Philos. Mag. 69:267-284.

[62] Smook J, Hamersma W, Pennings AJ (1984) The fracture process of ultra-high strength polyethylene fibres. J. Mater. Sci. 19:1359–1373.

[63] Hoogstein W, ten Brinke G, Pennings AJ (1988) DSC experiments on gel-spun polyethylene fibers. Coll. Polym. Sci. 266, 1003-1013.

[64] O'Connor TC, Robbins MO (2016) Chain Ends and the Ultimate Tensile Strength of Polyethylene Fibers. ACS Macro Lett 5:263-267.

[65] Bastiaansen CMW (1992) Tensile strength of solution-spun, ultra-drawn ultra-high molecular weight polyethylene fibres: 1. Influence of fibre diameter. Polymer 33:1649-1652.

[66] Strawhecker KE, Sandoz-Rosado EJ, Stockdale TA, Laird ED (2016) Interior morphology of high-performance polyethylene fibers revealed by modulus mapping. Polymer 103:224–232.

[67] Termonia Y, Meakin P, Smith P (1985) Theoretical Study of the Influence of the Molecular Weight on the Maximum Tensile Strength of Polymer Fibers. Macromolecules 18:2246-2252.

[68] Wang S, Shan Z, Huang H (2017) Mechanical Properties of Nanowires. Adv. Sci. 4:1600332.

[69] Lu Y, Song J, Huang JY, Lou J (2011) Fracture of Sub-20nm Ultrathin Gold Nanowires. Adv. Funct. Mater. 21:3982–3989

[70] Wang L, Liu P, Guan P et al (2013) In situ atomic-scale observation of continuous and reversible lattice deformation beyond the elastic limit. Nat. Commun. 4:2413.

[71] Vollrath F, Knight DP (2001) Liquid Crystalline Spinning of Spider Silk. Nature 410:541-548.

for Cover Art

Ultrafine High Performance Polyethylene Fibers

*Jay H. Park, and Gregory C. Rutledge**